Journal of Biomolecular NMR **29:** 151–166, 2004.

Side chain dynamics monitored by ^{13}C-^{13}C cross-relaxation

Klaartje Houben & Rolf Boelens*
Bijvoet Center for Biomolecular Research, NMR Spectroscopy, Utrecht University, Padualaan 8, 3584 CH Utrecht, The Netherlands

Received 30 September 2003; Accepted 10 December 2003

Key words: ^{13}C-^{13}C cross-relaxation, NOE, side chain dynamics, subtilisin PB92

Abstract

A method to measure ^{13}C-^{13}C cross-relaxation rates in a fully ^{13}C labeled protein has been developed that can give information about the mobility of side chains in proteins. The method makes use of the (H)CCH-NOESY pulse sequence and includes a suppression scheme for zero-quantum (ZQ) coherences that allows the extraction of initial rates from NOE buildup curves.

The method has been used to measure ^{13}C-^{13}C cross-relaxation rates in the 269-residue serine-protease PB92. We focused on C^{α}-C^{β} cross-relaxation rates, which could be extracted for 64% of all residues, discarding serine residues because of imperfect ZQ suppression, and methyl ^{13}C-^{13}C cross-relaxation rates, which could be extracted for 47% of the methyl containing C-C pairs. The C^{α}-C^{β} cross-relaxation rates are on average larger in secondary structure elements as compared to loop regions, in agreement with the expected higher rigidity in these elements. The cross-relaxation rates for methyl containing C-C pairs show a general decrease of rates further into the side chain, indicating more flexibility with increasing separation from the main chain. In the case of leucine residues also long-range C^{β}-C^{δ} cross-peaks are observed. Surprisingly, for most of the leucines a cross-peak with only one of the methyl C^{δ} carbons is observed, which correlates well with the χ_2 torsion-angle and can be explained by a difference in mobility for the two methyl groups due to an anisotropic side chain motion.

Abbreviations: ZQ – Zero-quantum; DQ – Double-quantum; NOE – Nuclear Overhauser Enhancement; NOESY – Nuclear Overhauser Enhancement Spectroscopy; TOCSY – Total Correlation Spectroscopy; CSA – Chemical Shift Anisotropy.

Introduction

Proteins, especially in solution, are not rigid but undergo a wide range of motions. These motions range from vibrational and torsional modes in the protein backbone and side chains to large conformational changes and local or global unfolding processes (Jardetzky and Roberts, 1981; Brooks et al., 1988; Frauenfelder, 2002). These motions are considered to play an important role in the biological function of proteins (Eisenmesser et al., 2002). NMR relaxation studies allow to characterize these motions over a wide range of frequencies (Peng and Wagner, 1994; Fischer et al., 1998; Palmer, 2001). In particular, ^{15}N relaxation rate analysis has been used to study the motion of the protein backbone in the ps-ns timeframe (Kay et al., 1989). Though side chain motions in certain residues can be characterized by ^{15}N relaxation as well (Boyd, 1995) more general methods use ^{13}C and ^{2}H relaxation measurements. Knowledge of side chain motions is particularly interesting because side chains are often involved in specific interaction with other molecules. Moreover, the degrees of freedom for motion are higher in the side chain than in the backbone. However, the study of motional properties of side chains is in general more complex. ^{13}C T_1 and T_2 auto-relaxation rates are more difficult to interpret as compared to ^{15}N relaxation rates, due to

*To whom correspondence should be addressed. E-mail: boelens@nmr.chem.uu.nl

C-C dipolar and scalar interactions in uniformly ^{13}C labeled proteins and by the occurrence of more than one proton in case of methylene and methyl groups. Both Yamazaki et al. (1994) and Engelke et al. (1995) performed ^{13}C relaxation studies in a fully labeled protein, but focused therefore on the relaxation of the backbone $^{13}C^{\alpha}$ nucleus. To simplify the ^{13}C relaxation properties studies have been performed at natural abundance (Nirmala and Wagner, 1988; Palmer et al., 1991), with carbon labeling at specific sites (Henry et al., 1986; Nicholson et al., 1992; LeMaster and Kushlan, 1996; Lee et al., 1997) or with random fractional ^{13}C labeling (Wand et al., 1995, 1996). In addition random fractional deuteration at a moderate level (LeMaster and Kushlan, 1996) can overcome the problem of having more than one ^{1}H attached to each ^{13}C nucleus. Measurement of deuterium T_1 and $T_{1\rho}$ relaxation times in $^{13}CH_2D$ methyl (Muhandiram et al., 1995; Kay et al., 1996) and ^{13}CHD methylene (Yang et al., 1998) groups has been demonstrated to be another method to measure side chain dynamics. This method has recently been extended by measuring five relaxation rates per deuteron (Millet et al., 2002; Skrynnikov et al., 2002). In addition cross-correlated relaxation rates (Ernst and Ernst, 1994; Engelke and Ruterjans, 1998; Yang et al., 1998; Banci et al., 2001; Carlomagno et al., 2003) can be used to probe side chain motions.

Here we propose to monitor side chain dynamics by measuring ^{13}C-^{13}C cross-relaxation rates for carbon nuclei in the side chain. In contrast to other methods these rates can be measured in a fully ^{13}C-labeled protein without need for deuteration. The relaxation mechanism is purely dipolar, with no CSA contribution, which makes it relatively easily to analyze. The two covalently bound carbons are at a well-defined distance and it is possible to extract dynamical information directly from the cross-relaxation rates. Previously both Zeng et al. (1996) and Cordier et al. (1996) showed that $^{13}C^{\alpha}$-^{13}CO cross-relaxation rates are indicative for the dynamics of the C^{α}-CO backbone vector. These rates were determined respectively by measuring the steady-state NOE in presence of a saturating field or the transient NOE by inversion of one of the spins. A drawback of measuring the steady-state NOE is that ^{13}C T_1 relaxation times have to be measured to extract the cross-relaxation rates σ. In case of a transient NOE between two carbon atoms the cross-relaxation rate can be obtained by measurement of the build-up of a ^{13}C-^{13}C NOE. We chose to measure the transient NOE using a HCCH-NOESY pulse sequence (Fischer et al., 1996) that was improved by introducing a suppression scheme for zero-quantum (ZQ) coherences. It is recorded as a 3D experiment to reduce problems of overlap and by changing the mixing time in the experiment the build-up of the C-C cross-peaks can be studied. Because the experiment is similar to the (H)CCH-TOCSY experiment used to assign carbon resonances in protein side chains, the (H)CCH-TOCSY peak assignments can directly be transferred to the (H)CCH-NOESY spectrum, which eases the analysis.

The pulse sequence was applied to the high-alkaline subtilisin PB92, an industrial enzyme used as a protein-degrading component in washing powders (Siezen et al., 1991). The structure of subtilisin PB92 (269 residues and a molecular weight of 27 kDa) has been determined by crystallography with a resolution of 1.8Å (1IAV) (Graycar et al., 1999) and compares well with those of several variants, such as savinase, for which several high resolution structures exist (1GCI 0.78 Å) (Kuhn et al., 1998). Also a solution structure of PB92 is known (Martin et al., 1997). A number of reasons led to the choice for this enzyme to be the focus of this ^{13}C-^{13}C cross-relaxation study. A large size, and thus relatively long rotational correlation time, would make the ^{13}C-^{13}C NOE more intense. Moreover the high number of residues and the existence of a detailed structure give the possibility to compare cross-relaxation rates of different amino acids with reasonable statistics in one system. A further advantage of this protein is that it tumbles highly isotropic in solution as was shown previously by ^{15}N relaxation data (Remerowski et al., 1996; Mulder et al., 1999).

We show that ^{13}C-^{13}C cross-relaxation rates in the side chains of a large number of residues can be obtained, with the exception of serine and threonine C^{α}-C^{β} and leucine C^{γ}-C^{δ} pairs, for which ZQ-suppression is not optimal. There is a general trend that C^{α}-C^{β} cross-relaxation rates are larger in stable secondary structure elements than in loop regions, as well as that ^{13}C-^{13}C cross-relaxation rates close to the backbone are higher than further into the side chain. This can be explained by the differences in dynamical properties at those locations in the protein. In addition we found that for the majority of leucines the long-range C^{β}-C^{δ} NOE cross-peaks are unequal for the two prochiral methyls, indicating that there can be differences in dynamics for these two methyls.

Material and methods

^{13}C-^{13}C cross-relaxation rate analysis

For a large molecule that tumbles isotropically in solution the cross-relaxation rate between two carbon spins is simply:

$$\sigma_{CC} = -d \cdot S^2 \tau_c, \quad (1)$$

where $d = \frac{1}{10}(\mu_0/4\pi)^2(\gamma_C^2\hbar/r_{CC}^3)^2$, μ_0 is the permeability constant of free space ($4\pi \times 10^{-7}$ kg m s^{-2} A^{-2}), γ_C is the carbon gyromagnetic ratio (6.73×10^7 rad s^{-1} T^{-1}), $\hbar$ is Planck's constant divided by $2\pi(1.05 \times 10^{-34}$ J s), r_{CC} is the distance between the two carbon spins ($\sim$1.54 Å), τ_c is the overall rotational correlation time and S^2 the generalized order parameter (Lipari and Szabo, 1982). The order parameter, which is an indicator of local flexibility, is in this case directly reflected in the cross-relaxation rate. This rate can be determined by measuring the transient NOE between two carbon spins. The build-up of magnetization on one carbon is equal to the NOE, $a_{CC}(t)$, times the initial magnetization ($\Delta I_z(0)$) on the second carbon. From the initial slope of the build-up curve the cross-relaxation rate can be extracted provided that the initial magnetization is known.

$$\lim_{t\to 0}\left(\frac{da_{CC}(t)}{dt}\right) = -\sigma_{CC}. \quad (2)$$

Sample preparation

Uniformly $^{15}N/^{13}C$ labeled subtilisin PB92 prepared as described in Fogh et al. (1995) and dissolved in D_2O containing 25 mM deuterated acetate buffer of pH 5, was used for all NMR experiments. All experiments were run at 315 K.

NMR experiments

In Figure 1 the (H)CCH-NOESY (Fischer et al., 1996) pulse sequence is shown. All spectra were recorded on a Bruker Avance 600 spectrometer equipped with a TXI probe with z-gradients (^{1}H frequency of 600.28 MHz). States-type sampling (States et al., 1982) was applied to obtain phase discrimination in indirect dimensions. To determine the optimum mixing time 2D H(C)(C)H-NOESY spectra were acquired with 16 scans using a spectral width of 7002.8 Hz in both dimensions and 350 × 512 complex points. (H)C(C)H-NOESY spectra with and without ZQ suppression were recorded with 32 scans, spectral widths of 13000.0 Hz × 12019.2 Hz and 180 × 1024 points.

To measure the NOE build-up five 3D (H)CCH-NOESY spectra were recorded with different mixing times (22 ms, 50 ms, 100 ms, 200 ms, 300 ms). The shortest mixing time used was 22 ms, because the ZQ filter, trim-pulses and gradient pulses had a total length of 13 ms and accordion incrementation (Bodenhausen and Ernst, 1982) of the mixing time by 200 μs increased the average mixing time by another 9 ms. The number of complex points and the spectral widths in the three dimensions were 90 × 50 × 1024 and 13000.0 Hz × 6000.0 Hz × 12000.0 Hz (C(f1) × C(f2) × H(f3)), respectively. The carrier was placed at 39 ppm and changed to 26 ppm before the t2 evolution period. Depending on the mixing time the experimental time ranged from 57 to 69 h using 8 scans for each experiment. For control the experiment was repeated, once without C' decoupling pulses during t1 and t2 and once without these pulses and the ^{13}C carrier at 20 ppm without any offset jump.

To compare the sensitivity of a (H)CCH-NOESY spectrum with a (H)CCH-TOCSY spectrum, a 3D (H)CCH-TOCSY (Bax et al., 1990) spectrum was recorded with a short DIPSI3 (Shaka et al., 1988) cycle of 7.8 ms, using the same number of points and spectral widths as described above.

A 3D ^{1}H detected long-range ^{13}C-^{13}C correlation spectrum was recorded as described by Bax et al. (1992), using the same spectral widths as reported for the 3D (H)CCH-NOESY spectra and 110 × 55 × 1024 points. In addition a constant-time ^{13}C-HSQC was recorded with 300 × 1024 points and a constant time period of 13.3 ms. These two spectra were both recorded on a Bruker Avance 600 spectrometer that is equipped with a cryoprobe and were used to determine long-range $^3J_{C\alpha C\delta}$ coupling constants in leucine residues.

All spectra were processed using the NMRPipe software package (Delaglio et al., 1995). In both indirect dimensions a 0.45π shifted squared sine-bell window function was used and for the acquisition dimension a 0.45π shifted sine-bell was used. All dimensions were zero-filled twice. The spectra were analyzed using NMRView (Johnson and Blevins, 1994).

To estimate differential scaling of NOEs due to differential proton R_1 relaxation rates during the recycle delay, three 3D (H)CCH-NOESY spectra were measured with different values for the recycle delay of 0.5, 0.75 and 1.1 s, using a NOE mixing time of 300 ms. Cross-peak intensities were fitted to the equation $I = I^{eq.} \cdot (1 - \exp[-R_1(RD+AQ)])$ (Cain et al.,

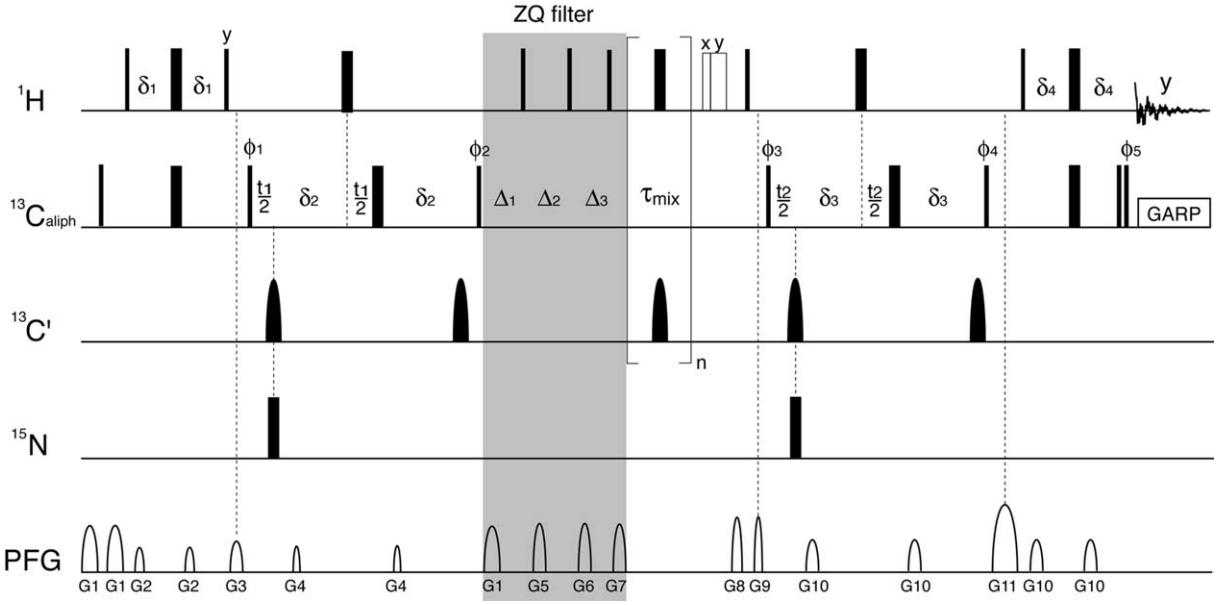

Figure 1. (H)CCH-NOESY pulse sequence used to measure ^{13}C-^{13}C cross relaxation rates. Filled narrow and wide bars correspond to squared high power 90° and 180° pulses, respectively. All pulses are applied along the x-axis with a field strength of 22.7 kHz, unless indicated otherwise. The two open bars represent two trim pulses to dephase residual water of 1 and 2ms, respectively. The ^{13}C was at 39 ppm and ^{13}C' pulses were applied as low power (2.3 kHz) Gaussian shaped pulses with an offset of 139 ppm. The applied pulsed field gradients are sine shaped using a shape of 100 points. The following delays were used: $\delta1 = \delta4 = 1.6$ ms, $\delta2 = \delta3 = 1.1$ ms, $\Delta1 = 3.6$ ms, $\Delta2 = 1.8$ ms, $\Delta3 = 1.2$ ms. On the last line the gradients are indicated; G1: 500 μs, 77%; G2: 500 μs, 1.6%; G3: 2000 μs, 30%; G4: 300 μs, 2.7%; G5: 1000 μs, 93%; G6: 1000 μs, 73%; G7: 300 μs, 85%; G8: 1000 μs, 15%; G9: 440 μs, 15%; G10: 500 μs, 2.7%; G11: 2000 μs, 100%. The phase cycle was as follows: $\phi1 = x,-x$; $\phi2 = y$; $\phi3 = 2(y),2(-y)$; $\phi4 = x$; $\phi5 = 4(x),4(-x)$; $\psi rec = x,-x,-x,x$. Quadrature detection in t1 and t2 was achieved by incrementing ϕ1 and ϕ4 respectively together with the receiver phase according to the States method. During acquisition a GARP decoupling sequence is applied with 3 kHz field strength.

1996), where RD is the recycle delay and AQ the acquisition time. In addition differential transversal relaxation losses during the INEPT steps of the 3D (H)CCH-NOESY experiment were estimated by recording experiments with increasing lengths of the INEPT periods. For δ1 an extra delay with a proton 180° in the middle was added just before the second ^{1}H 90° pulse (Figure 1). Two extra 3D (H)CCH-NOESY spectra were recorded in this way, using a delay of 0.4 and 2.0 ms, respectively. Similarly an extra delay with a carbon 180° in the middle was placed just before the second ^{13}C 90° pulse, to estimate relaxation losses during δ2. Another two 3D (H)CCH-NOESY spectra were acquired with two different values, 0.4 and 2.0 ms, for the inserted delay. From a linear fit of the cross-peak intensities the relaxation losses during δ1 and δ2 were estimated for a group of C^β-C^α cross-peaks. The estimated differential losses are assumed to be the same for δ1 and δ4 and δ2 and δ3 (Figure 1). This will not give an underestimation but rather an overestimation of the differential cross-peak scaling, since the proton and carbon T_2 times will vary more among H^β and C^β nuclei, on which the magnetization resides during δ1 and δ2, than for H^α and C^α nuclei.

Data analysis

Peak volumes in the five 3D spectra were obtained using the standard integration routine of NMRView (Johnson and Blevins, 1994). These volumes were corrected for different INEPT transfer efficiencies caused by differences in $^1J_{CH}$ coupling constants and losses due to $^1J_{CC}$ coupling during the evolution periods (see Supplementary Material). To be able to extract order parameters from the relaxation data, volume normalization for alanine C^α-C^β cross-peaks was also done in another way. The volumes of four free C^α-C^α and six free C^β-C^β diagonal peaks were extrapolated to 0 ms and averaged and a normalization factor was computed as the square root of the product of the two average diagonal volumes.

The build-up curves were fitted to a fit function described by Equation 3 using Gnuplot 3.7 (http://www.gnuplot.info) with the NLLS (non-linear

least-square) Marquardt–Levenberg routine in that program,

$$f(t) = -\sigma t \cdot e^{-\rho t} + A, \quad (3)$$

where σ is the cross-relaxation rate, ρ the longitudinal auto-relaxation rate and A an offset-correction term. Errors in σ and ρ are obtained from the asymptotic standard errors generated by Gnuplot. Because we are only interested in the initial slope of the build-up curves, the data were fitted using a simple exponential ($e^{-\rho t}$) for the decay function. The cross-relaxation rates thus determined are in a.u.

Results and discussion

Pulse sequence

The pulse sequence used to measure the ^{13}C-^{13}C cross-relaxation rates is shown in Figure 1 and was based on the previously published (H)CCH-NOESY sequence by Fischer et al. (1996). During the ^{13}C evolution period before the mixing time the C-C scalar coupling is active and coherences like $C_y^1 C_z^2$ are created that could give rise to dispersive anti-phase cross-peaks that may interfere with estimating the NOE cross-peak intensities, especially at short mixing times. During the mixing time these $C_y^1 C_z^2$ coherences become $C_y^1 C_x^2$, a combination of ZQ and DQ coherences. The DQ part can easily be dephased by strong pulsed field gradients, but because of their low frequency the ZQ coherences cannot be dephased by a field gradient. Two subsequent methods to suppress these ZQ coherences are applied in this pulse sequence. First a 'ZQ-filter' was placed in the beginning of the mixing time. This filter consists of a delay followed by a 90° proton pulse and a field gradient pulse. During the delay the one bond ^1H-^{13}C scalar coupling is active, which will result in a coherence like $C_x^1 H_z^1 C_y^2 H_z^2$. The following 90° proton pulse will create a heteronuclear MQ coherence, which will further dephase by subsequent gradient pulses depending on both carbon and proton frequencies. This sequence is repeated three times with three different delays ($1/(2J_{CH})$, $1/(4J_{CH})$, $1/(6J_{CH})$) optimized for methyne, methylene and methyl groups, respectively. As a second method the mixing time is incremented in a proportion χ to t_1, as in 2D accordion spectroscopy (Bodenhausen and Ernst, 1982; Rance et al., 1984). The ZQ cross-peak will be split along the f1 axis by $\pm(\Omega_1 - \Omega_2)\chi$ and will thus appear as side bands of the NOE cross-peak. It is very important to suppress these ZQ coherences, first because they bias the cross-peak intensities at short mixing time and second because they are, in contrast to the wanted magnetization C_z, susceptible to CH-CH dipole dipole cross-correlated relaxation effects.

2D (H)C(C)H-NOESY spectra with and without ZQ suppression using a short mixing time were recorded to see the effect of the ZQ suppression. Figure 2A shows the spectral region with correlations between the C^β and the H^α resonances. The high intensities are due to ZQ effects. In Figure 2B these ZQ coherences are strongly suppressed, using the two filters described above. However, both methods used for ZQ suppression depend on the difference in frequencies of the involved nuclei. In cases where both the ^{13}C and the ^1H frequencies are very similar, such as for $C^\alpha \leftrightarrow C^\beta$ cross-peaks of serines or $C^\gamma \leftrightarrow C^\delta$ cross-peaks of leucines, the ZQ frequency will be close to zero, making it hard to suppress or displace artifacts due to ZQ coherences. In Figure 2C and 2D can be seen that the $C^\beta \rightarrow C^\alpha$ cross-peak of serine 206 (with a ZQ frequency of approximately 400 Hz) is not affected by either the ZQ filter or incrementation of the mixing time.

The value of the cross-relaxation rate between carbon and the directly attached proton is opposite in sign and similar in size as the ^{13}C-^{13}C cross-relaxation rate. During the mixing time ^{13}C-^1H cross-relaxation is suppressed by applying 180° proton pulses every 10 ms. It is important to suppress ^{13}C-^1H cross-relaxation, because in this way the indirect transfer of magnetization via the ^1H-^1H NOE ($C^1 \rightarrow H^1 \rightarrow H^2 \rightarrow C^2$) is also suppressed. In the same way cross-relaxation between C^α and C' is suppressed by applying 180° pulses on carbonyl. These pulses are given every 50 ms. No pulses are given on nitrogen because cross-relaxation between carbon and nitrogen is negligibly slow.

Several 2D H(C)(C)H- and (H)C(C)H-NOESY spectra were recorded to test the pulse sequence. From a set of 2D H(C)(C)H-NOESY spectra the optimum mixing time in terms of intensity was determined to be around 500 ms (Figure 3). To stay close to the linear part of the build-up curve mixing times ranging from 0–300 ms were used to determine the NOE build-up. Figure 4 shows two ^1H 1D traces from the 3D spectrum with a mixing time of 300 ms compared to the same traces of a 3D (H)CCH-TOCSY with a short DIPSI3 cycle of 7.8 ms. For this protein the NOESY is a factor 3 to 5 less sensitive than the TOCSY.

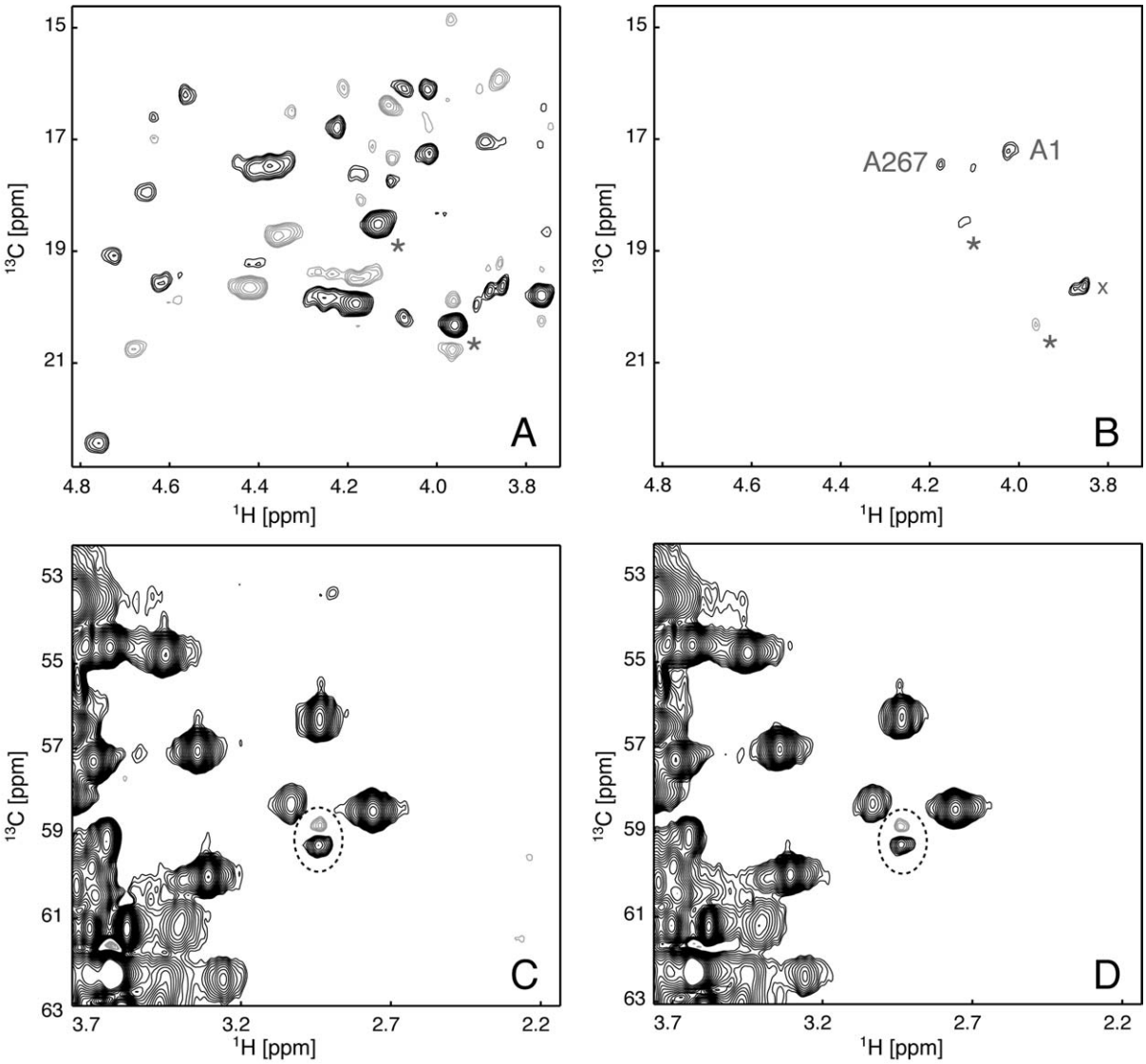

Figure 2. Expansions of the 2D (H)C(C)H-NOESY spectrum of subtilisin PB92 with short mixing time. A and C are recorded without ZQ suppression, B and D with ZQ suppression. Black is used for positive contour levels and grey for negative contour levels. (A, B) In the selected region alanine C^{β}-C^{α} NOE cross-peaks will appear at longer mixing times. The peaks that occur in spectrum A originate from ZQ coherences, which are well suppressed in spectrum B. The remaining peaks are marked. Two peaks are NOE cross-peaks for alanine 1 and 267. The peaks marked with a * are not fully suppressed ZQ peaks and the peak marked with a x is an artifact from a nearby strong diagonal peak. The unmarked peak is most probably noise. (C, D) In addition to 'diagonal' peaks, the C^{β}-C^{α} NOE cross-peak of S206 will appear at longer mixing times at the position, which is denoted with the dashed circle. However, the cross-peak seen here is not NOE mediated, but originates from a ZQ coherence, which cannot be suppressed because of the low C^{β}-C^{α} ZQ frequency, as seen in spectrum D.

Normalization

As described above the cross-peak intensity is dependent on the NOE build-up times the initial magnetization. In order to determine the absolute values for the cross-relaxation rates, the initial magnetization should be known. In addition the loss of magnetization in the part of the pulse sequence after the mixing time should be taken into account. In other words the peak volumes should be normalized. The square root of the product of the two diagonal peak volumes at zero mixing time belonging to the involved nuclei would be a proper factor to use for the normalization of the peak volumes, because of the symmetry of the pulse sequence. However, strong overlap on the diagonals

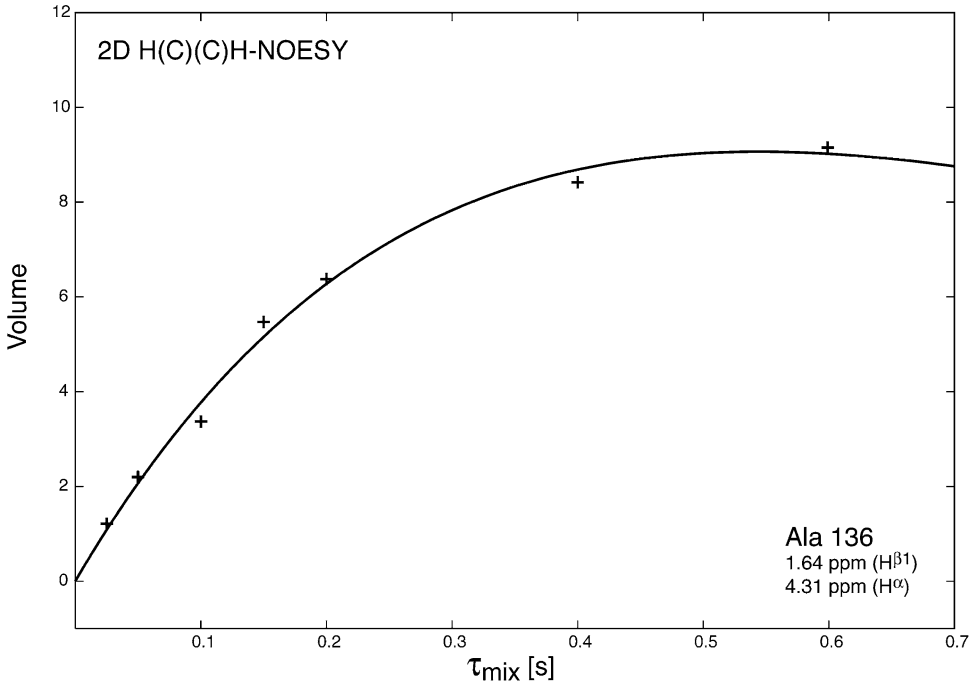

Figure 3. Build-up of the C^{α}-C^{β} cross-peak of Ala136 in a 2D H(C)(C)H-NOESY spectrum of subtilisin PB92. The maximum intensity is reached for a mixing time between 0.5 s and 0.6 s.

in 3D spectra of large proteins makes it problematic to accurately determine the diagonal peak volumes. Therefore we chose an approximate method, where we correct the initial magnetization numerically.

The cross-peak intensities will vary because of differences in the efficiency of magnetization transfer during the various INEPT steps and evolution periods. Factors modulating the efficiency are the active and passive coupling constants ($^1J_{HH}$, $^1J_{CH}$, $^1J_{CC}$) and the T_2 relaxation times of the involved coherences. The H-H coupling constants are less than 15 Hz, thus with a delay of 3.2 ms and coupling to 3 protons the loss of magnetization is only 4% and can be neglected. Both the C-C (Bystrov, 1976) and C-H (Zwahlen et al., 1997) coupling constants are known to good approximation and correction factors can be used to correct for differences in intensity loss during the INEPT periods. Differential losses of magnetization due to T_2 relaxation during these periods can cause differences in cross-peak intensities. To estimate the error that is introduced by this we recorded spectra with varying lengths of the INEPT steps as is described in the methods section. In this way only a crude estimation of the differential relaxation losses could be obtained and therefore these numbers are not suitable to properly normalize the individual cross-peak intensities. However, they provide an estimation for the error that is introduced not correcting for differential relaxation losses. The scaling factor computed in this way has a value of 0.31 with a standard deviation of 0.07. Also the steady state magnetization, which depends on the T_1 relaxation time of the involved ^1H and thus the length of the recycle delay, affects the cross-peak intensities. If the recycle delay would be three times the longest T_1 time, all proton magnetization would be back to equilibrium before the next cycle, which would prevent differences in initial magnetization. But in practice this is not feasible, because the experimental time for a 3D experiment would become unrealistically long. Therefore a shorter recycle delay of 1.1 s was used. As known from literature, the proton T_1 relaxation times mainly differ between different kind of protons, i.e., 0.7, 1.4 and 1.8 s for methyl, alpha and aromatic protons respectively (Cavanagh et al., 1996). When comparing cross-peaks for the same C-C pair in different amino acids, this should not cause any substantial difference. However, it could lead to differences between the cross-peaks at either side of the diagonal, because they are observed at different protons. To estimate the differential scal-

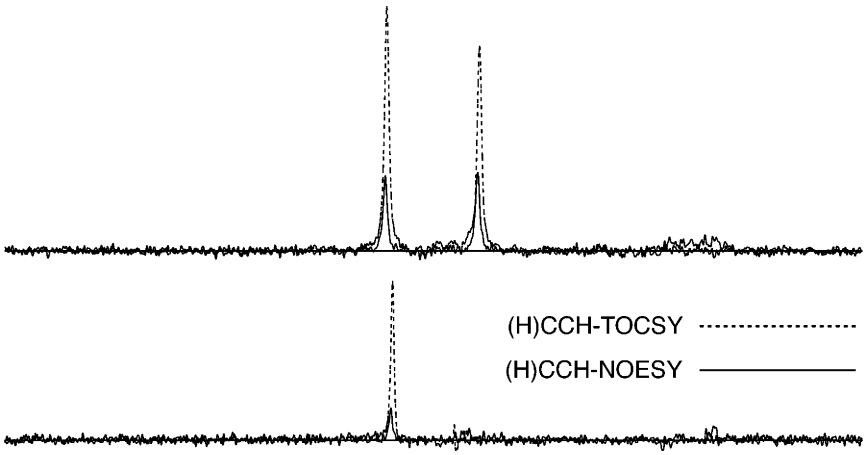

Figure 4. Comparison of the sensitivity of the (H)CCH-NOESY experiment to the (H)CCH-TOCSY experiment. Two ^{1}H 1D traces from the 3D (H)CCH-NOESY spectrum with a mixing time of 300 ms (filled line) are shown with the same traces from a 3D (H)CCH-TOCSY with a short DIPSI3 cycle of 7.8 ms (dashed line). The upper trace displays two C^{α}-C^{β} cross-peaks from Thr214 and Tr218 and the lower trace a C^{α}-C^{β} cross-peak from Ile77. On average the NOESY experiment is a factor 3 to 5 less sensitive than the TOCSY for this protein.

ing of cross-peak intensities due to differential proton T_1 relaxation times, we recorded three experiments with different recycle delays, giving an average scaling factor of 0.82 with a standard deviation of 0.14. Combining the effect of relaxation during the INEPT delays and the effect of non-equilibrium steady state magnetization we found that the volumes of 72 C^{β}-C^{α} cross-peaks are scaled by an average factor of 0.26 with a standard deviation of 0.07, which introduces an error of 28%.

C^{α}-C^{β} cross-relaxation rates

The cross-peaks in the 3D (H)CCH-NOESY spectra were assigned using the resonance assignments previously determined in our lab (Fogh et al., 1995). Figure 5A shows the build-up of two C^{α}-C^{β} NOE cross-peaks of Ala71, one observed at the H^{α} and the other at the H^{β} resonance frequency. The line widths of the two cross-peaks differ because of differences in T_2 of the observed protons. Therefore we chose to use volumes instead of intensities to measure the build-up of magnetization. Figure 5B shows such build-up curves of both the C^{α}-C^{β} and C^{β}-C^{α} cross-peaks of Ala71.

Figure 6 shows $C^{\beta} \rightarrow C^{\alpha}$ cross-relaxation rates corrected for multiplicity and differences in $^{1}J_{CC}$ and $^{1}J_{CH}$ coupling constants for 67% of the residues in the protein (see Supplementary Material to be obtained from the author), discarding serine residues because of insufficient suppression of ZQ coherences in most cases. In cases of overlap, imperfect ZQ suppression or low signal to noise peak volumes could not properly be determined. We only used cross-relaxation rates determined using the $C^{\beta} \rightarrow C^{\alpha}H^{\alpha}$ cross-peaks, since the magnetization transfer is not divided over two different cross-peaks, as is the case for some of the corresponding $C^{\alpha} \rightarrow C^{\beta}H_2^{\beta}$ cross-peaks. Note that since the data points only go up to 300 ms, the values for the decay term ρ have relative large errors. Carbon R_1 relaxation rates have been determined for a set of free peaks for this protein (data not shown) and range from 0.9–2.0 and 1.1–5.0 s^{-1} for the C^{α} and C^{β} nuclei, respectively. From this the decay term for the build-up curves could vary from 1.0–3.5 s^{-1}, which reasonably well agrees with the fit values that are found for the ^{13}C-^{13}C NOE build-up curves.

On average, residues that are located in secondary structure elements show faster cross-relaxation, indicating more rigidity. The differences in values between secondary structure elements and loop regions are however less pronounced than the differences in $\{^{1}H\}$-^{15}N NOE values. It is difficult to compare the ^{13}C-^{13}C cross-relaxation rates, obtained in this study, in detail with ^{15}N relaxation data, as obtained for the same protein previously (Mulder et al., 1999). Most of the residues in PB92 that are located in flexible loops are serines and glycines. For these serine residues no reliable values can be obtained due to overlap or non-suppressed ZQ coherences and for glycines we obviously have no ^{13}C-^{13}C cross-relaxation data. For the few remaining residues (Val102, Thr141 and Ala188) we found no low values for the C^{α}-C^{β} cross-

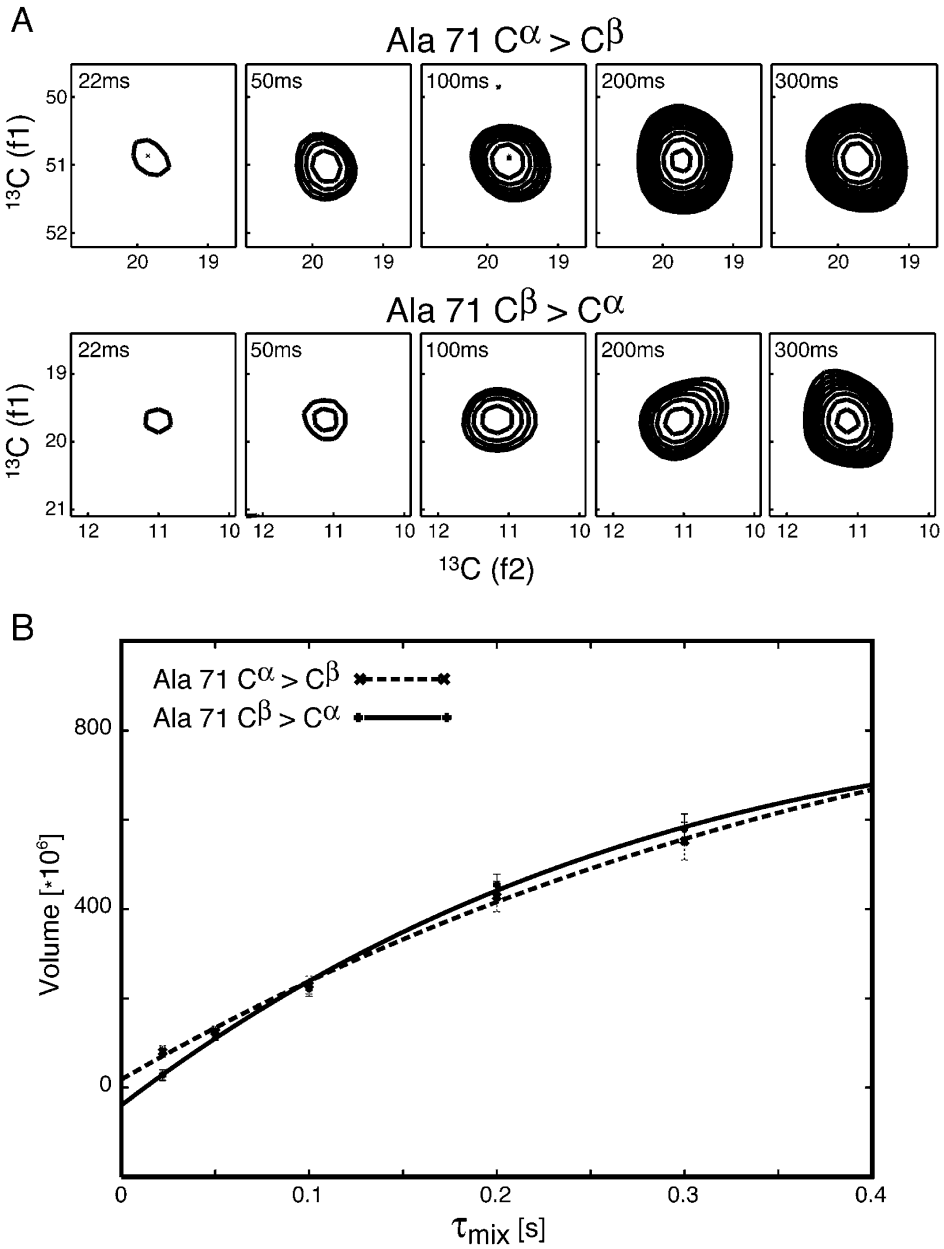

Figure 5. Build-up of cross-peak intensity by cross-relaxation between two carbon nuclei. (A) Expansion of a ^{13}C-^{13}C plane of 3D (H)CCH-NOESY spectra with different mixing times, showing the $C^{\alpha} \rightarrow C^{\beta}$ and the $C^{\beta} \rightarrow C^{\alpha}$ cross-peaks of Ala 71 respectively. (B) Build-up curve of the two cross-peaks from (A).

relaxation rates, indicating a lower dynamics for these residues then deduced from the ^{15}N relaxation data.

Figure 7 shows the cross-relaxation rates for alanine C^{α}-C^{β} pairs normalized using the diagonal volumes as described in the experimental methods. The rates determined in this way are in Hz. The scale on the right axis, that uses Equation 1, is in ns and represents the product of the overall rotational correlation time (τ_c) and the generalized order parameter (S^2), which corresponds to the methyl-axis order parameter (S^2_{axis}) that is often reported for methyl groups. From ^{15}N relaxation data the overall correlation time of subtilisin was estimated to be 7.6 ns in water at 315 K. However, the measurements here were performed in

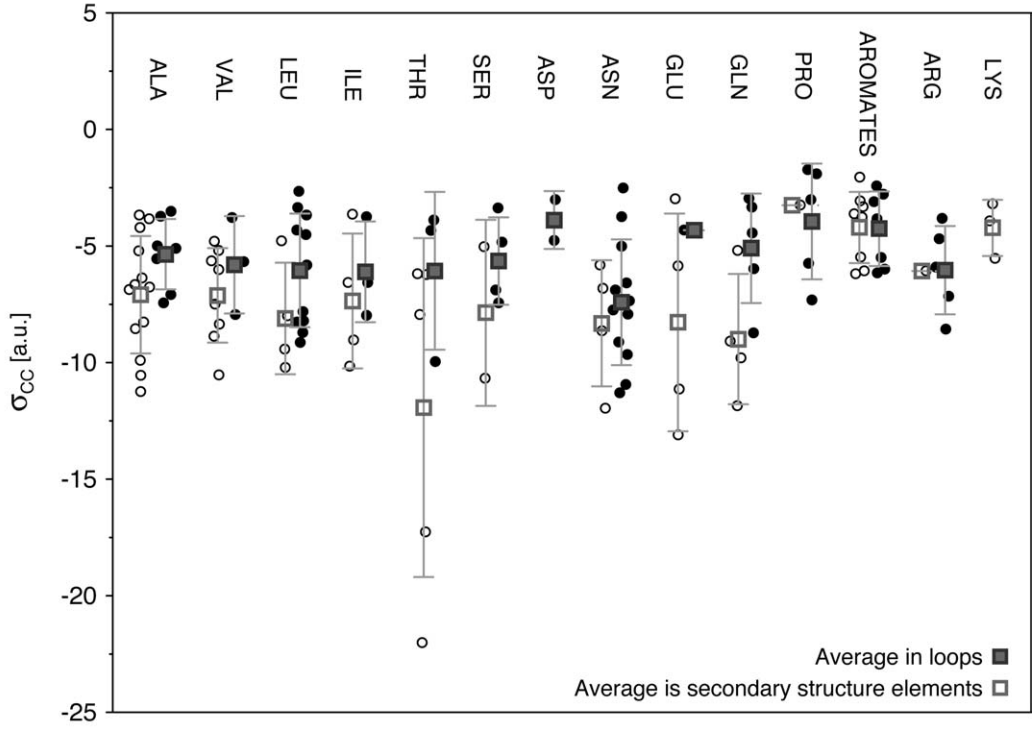

Figure 6. $C^{\beta} \rightarrow C^{\alpha}$ cross relaxation rates for most residues in subtilisin PB92. The open and filled circles indicate residues located in secondary structure elements or else in the structure, respectively. Open and filled squares give the average cross relaxation rate. On average residues that are located in secondary structure elements have higher absolute values for the cross-relaxation rates, which indicates rigidity.

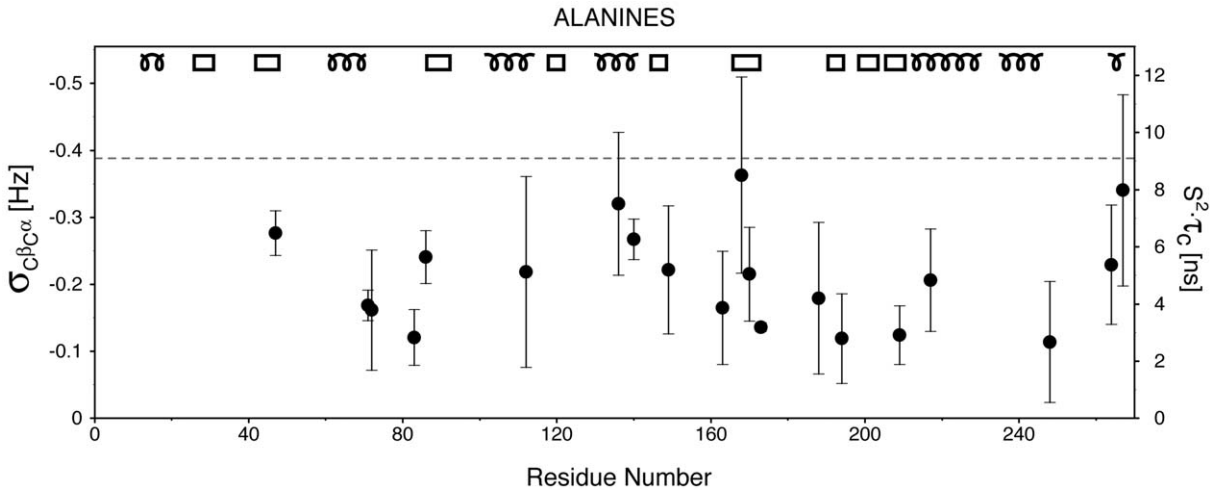

Figure 7. Cross-relaxation rates for alanine residues in subtilisin PB92. $C^{\beta} \rightarrow C^{\alpha}$ cross-peak volumes for most alanines in PB92 were normalized using the square root of the product of the two average diagonal volumes at 0 mixing time. Following Equation 1 the cross-relaxation rates obtained can be considered to be directly proportional to $S^2\tau_c$. The left axis gives the cross-relaxation rates in Hz and the right axis the corresponding values for $S^2\tau_c$ in ns using Equation 1. The blocks and curls at the top of the Figure indicate the positions of β-strands and helices, respectively. The dashed line is positioned at the approximate overall correlation time of PB92 for these experiments.

D_2O that is known to be a factor of 1.2 times more viscous than water at this temperature (Cho et al., 1999). The correlation time is proportional to the viscosity of the solvent giving an estimate of 9.1 ns, which is represented by the dotted line in Figure 7. The correlation times determined for the alanine residues in this study range from 2.7 to 8.5 ns, corresponding to order parameters between 0.3 and 0.9, with an average of approximately 0.5, a value that is significant lower than order parameters generally found for N-H atom pairs (S^2_{NH}) and C^α-H (S^2_{CH}). Mittermaier et al. (1999) made a histogram of alanine deuterium relaxation-derived methyl axis order parameters (S^2_{axis}) of eight different proteins and showed that the average value is close to 0.8, a value considerably higher than what we find. The correlation of backbone S^2_{NH} and alanine S^2_{axis} values was found to be poor, like in our study, however a similar distribution of S^2_{NH} and S^2_{axis} was found and ranges from 0.5 to 1.0. But in other methyl relaxation studies (Muhandiram et al., 1995; Yang et al., 1998; Lee et al., 1999; Loh et al., 2001; Walsh et al., 2001) values for alanine methyl axis order parameters are found that range from even 0.25 to 1.0.

The spread in C^β-C^α cross-relaxation rates shown in Figure 6 is higher than what is generally found from ^{15}N relaxation parameters and $^{13}C^\alpha$ relaxation studies. But as has already been noted by others for alanine residues for which methyl axis order parameters have been determined, the C^α-C^β axis not necessarily shows the same motional behavior as the N-H and C^α-H vectors (Walsh et al., 2001). Several studies have shown that the order parameters decrease going further into the side chain (LeMaster and Kushlan, 1996; Ramirez-Alvarado et al., 1998). The order parameters for the C^α-H^α bond vector have been found to vary from 0.5–1, with an average value of 0.8–0.9 (Mispelter et al., 1995; LeMaster and Kushlan, 1996; Wand et al., 1996). Order parameters for C^β-H bond vectors are tabulated less frequently, but ranged from 0.3–0.9 (Mispelter et al., 1995; LeMaster and Kushlan, 1996) from ^{13}C relaxation studies and 0.1–1 from ^2H relaxation studies (Yang et al., 1998) with an average value of 0.5. Methyl axis C^α-C^β order parameters are available for alanine residues and ranged from 0.25–1.0 with an average value around 0.8. A paper of Carlomagno et al. (2003) recently showed that order parameters for the C^α-C^β bond-vector can be determined from CH-CH cross-correlated relaxation provided that the χ_1 angle is known. The order parameters determined in this way ranged from 0.5 to $\geq$1 for Thr, Val and Ile residues. The C^β-C^α cross relaxation rates in this study range from -1.7 to -13, except for the extreme values for two Thr residues, which would roughly correspond to order parameters ranging from 0.13 to 1. From what is discussed above these values seem to be reasonable, but partially the scatter in cross-relaxation rates will also be caused by the error that is introduced by not correcting for differential relaxation losses during the pulse sequence. Engelke and Rüterjans (1998) measured ^{13}C heteronuclear NOE and T_1 for $C^\beta H$ and $C^\beta H_2$ groups and cross-correlated cross-relaxation rates for $C^\beta H_2$ groups in ribonuclease T1 and used a model of restricted rotational diffusion around χ_1 to extract motional parameters from these relaxation rates. They found that the motion of most groups can be characterized by an angular amplitude between 0° and 50° and an internal correlation time in the range of 100–800 ps. This also indicates that a wide range of motions can be present.

The lowest cross-relaxation rates are found for two proline residues, Pro129 and Pro162. The first proline is located in one of the flexible loops and high C^α and C^β B-factors are found for this residue in the crystal structure (1GCI). Pro162 however, has low B-factors in the crystal structure, but is located close to the weak (mM) Ca^{2+} binding site, where the carbonyl of Ala163 is a direct ligand to this ion. In our NMR sample no additional Ca^{2+} was added and this might be the reason for the increased dynamics. ^{15}N relaxation studies also showed variable and weak, but increased dynamics in this region of the protein (Mulder et al., 1999).

In Figure 6 two threonine residues (Thr214 and Thr218) have very high absolute cross-relaxation rates. From the data we have for the alanine residues we know that a cross-relaxation rate of approximately -13 corresponds to an order-parameter of 1. This would mean that the values found for Thr214 and Thr218 are unrealistically high, but nevertheless, they must be among the most rigid C^α-C^β vectors. These two threonines are both located in helix 5, which sticks through the interior of the protein and contains the active site Ser215. This active site has the same conformation in almost all subtilisins and appears to be extremely rigid (Siezen et al., 1991; Siezen and Leunissen, 1997). It appears that Thr214 and Thr218 reflect this high rigidity as well. The amide proton H^N and both the proton $H^{\gamma 1}$ and oxygen $O^{\gamma 1}$ of the hydroxyl group of Thr214 are involved in a hydrogen bond. For Thr218, which is more located towards the

interior of the protein, only the hydroxyl proton is involved in a hydrogen bond. Also three other threonine residues (Thr64, Thr132 and Thr141) that are all located in helices show strong C^{α}-C^{β} cross-peaks, but their cross-relaxation rates are not shown in Figure 6. This is because their cross-peaks either resonate close to the diagonal or show strong ZQ contributions in the short mixing time spectra, preventing their precise cross-relaxation rates to be extracted. However, when comparing the cross-peak volumes of several threonine residues in the 300 ms spectrum, where the ZQ contribution is negligible, it shows that these residues still have very high cross-peak intensities, indicating that the C^{α}-C^{β} bond vectors of these residues are on average more rigid than of the other threonines, for which we could measure $C^{\beta} \rightarrow C^{\alpha}$ rates. It is interesting to note that of these three other threonines Thr64 is located in the same helix as the active site residue His62.

C^{β}-C^{γ} and C^{γ}-C^{δ} cross-relaxation rates

In order to determine whether there is a correlation between ^{13}C-^{13}C cross-relaxation rates and the distance from the main chain, cross relaxation rates of C^{β}-C^{γ} and C^{γ}-C^{δ} pairs were measured and compared to the C^{α}-C^{β} rates. Because of their high sensitivity and because their NOEs are not divided over two cross-peak positions as is the case for methylene groups, we mainly focused on methyl containing C-C pairs. C^{β}-C^{γ} cross-relaxation rates could be determined for both threonines and valines (Figure 8). In case of isoleucines both C^{β}-$C^{\gamma 2}$ and $C^{\gamma 1}$-C^{δ} rates were extracted from the NOE build-up curves. Unfortunately, no direct data for leucine C^{γ}-C^{δ} pairs could be obtained due to the similarity in the C^{γ} and C^{δ} frequencies. In three cases C^{β}-C^{γ} cross-relaxation rates could be determined for both valine methyls. Their values do not differ more than 13%, which is the same range as the difference in methyl axis order parameters of up to 0.1 that is found by others (Nicholson et al., 1992; LeMaster and Kushlan, 1996; Mittermaier et al., 1999).

On average it can be seen that the spread in relaxation rates reduces going from C^{α}-C^{β} rates to C^{γ}-C^{δ} rates. The C^{β}-C^{γ} cross-relaxation rates of threonines are in most cases lower than the corresponding C^{α}-C^{β} cross-relaxation rates, indicating higher flexibility further into the side chain. Though this is not generally true for individual hydrophobic valine and isoleucine residues, the average cross-relaxation rates reduces with increasing distance from the main chain. When comparing cross-relaxation rates of different C-C pairs, such as C^{α}-C^{β} and C^{β}-C^{γ}, it should be kept in mind that these most likely are scaled in a different way because of difference in ^{13}C T_2 and ^{1}H T_1 relaxation. Earlier studies of both ^{2}H and ^{13}C relaxation parameters showed also a correlation of increased

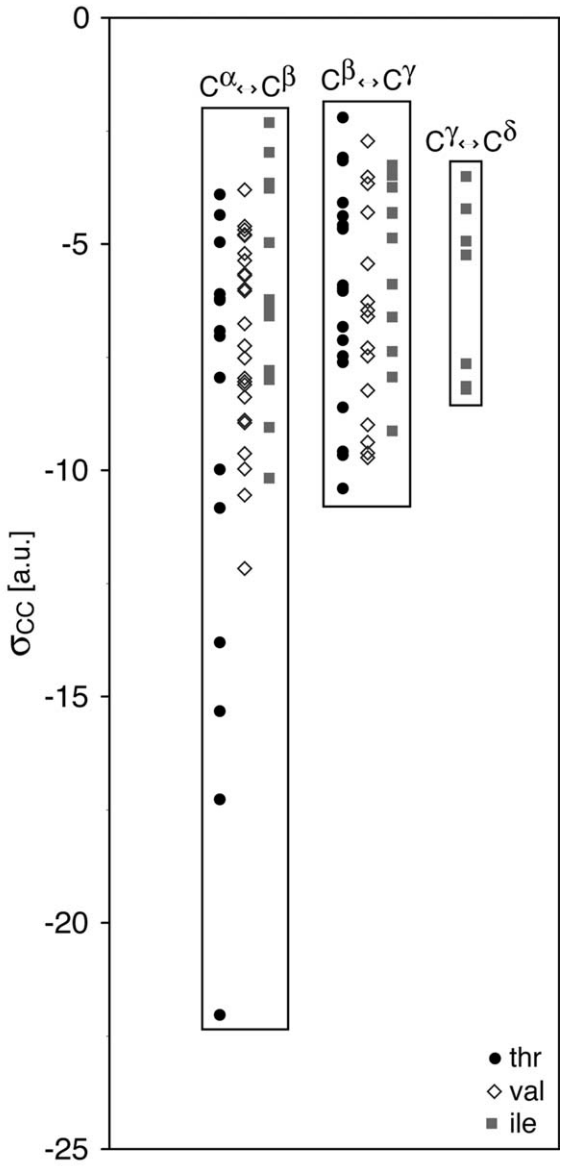

Figure 8. Cross-relaxation rates in arbitrary units for the side chains of threonine (C^{α}-C^{β} & C^{β}-$C^{\gamma 2}$), valine (C^{α}-C^{β} & C^{β}-$C^{\gamma 1/2}$) and isoleucine (C^{α}-C^{β}, C^{β}-$C^{\gamma 2}$ & $C^{\gamma 1}$-C^{δ}) residues. It shows that on average the cross-relaxation rates decrease when going further into the side chains. This indicates that there is higher mobility with increasing distance from the main chain.

mobility with the number of dihedral angles removed from the backbone (LeMaster and Kushlan, 1996; Mittermaier et al., 1999).

Long-range cross-peaks

For some residues, ^{13}C-^{13}C NOE cross-peaks over a distance longer than 1.54 Å could be observed, showing up in spectra with a mixing time of 100 ms or longer. This was the case for some of the threonines and most of the leucines for which respectively C^{α}-C^{γ} and C^{β}-C^{δ} and $C^{\delta 1}$-$C^{\delta 2}$ cross-peaks were identified. In all cases it involves methyls, presumably because of their high sensitivity in the 3D (H)CCH-NOESY experiment. In contrast these long-range cross-peaks were not found, or only very weakly, for valines and isoleucines. Since the direct transfer over 2.55 Å is roughly 5–10 times less efficient than the spin diffusion pathway, these long-range cross-peaks are most probably mediated by spin-diffusion via C^{β} for threonines and via C^{γ} for leucines. No other carbon nuclei are in closer proximity (>3 Å) than the covalently attached carbon, excluding other spin diffusion pathways.

For 16 out of 19 leucine residues a C^{β}-C^{δ} cross-peak on the H^{δ} protons was observed. An interesting phenomenon is that of these 16 in 12 cases only one of the two cross-peaks is observed (see Table 1). To make sure that these differences are not caused by the experimental set-up, two 3D spectra were recorded, one where the carbonyl shaped pulses were omitted and one with both the ^{13}C offset in the methyl region and no carbonyl pulses. Both spectra show the same behavior, excluding the differences to be originating from experimental artifacts. We should also exclude that these differences are caused by other relaxation pathways, like CH-CH dipole dipole cross-correlated relaxation or ^{1}H-^{1}H NOE. The wanted relaxation C_z is not affected by these processes, however ZQ coherences that are present after the last ^{13}C pulse before the mixing time are susceptible to these processes. However, from the 3D spectrum with short mixing time (22 ms) can be seen that there are no contributions to the cross-peaks from ZQ coherences. In addition CCH-NOESY spectra (data not shown), where the first INEPT step is omitted, show the same behavior for the C^{β}-C^{δ} cross-peaks. The period in which the $^{1}J_{CC}$ can evolve is much shorter for this experiment (0.27 ms + t1 vs. 2.23 ms + t1; t1-max = 3.73 ms), which confirms that these cross-peaks do not originate from J transfer, but from NOE transfer. Additionally we can exclude that passive C-H couplings in case of CH_2 and CH_3 groups would contribute to the observed differences, because there is no $^{1}J_{CH}$ coupling evolution before the NOE mixing time in the case of the CCH-NOESY experiment. The ^{1}H-^{1}H NOE can cause a problem if we do not properly cancel cross-relaxation between ^{13}C-^{1}H, because in that case magnetization could be transferred to other carbon nuclei via their attached protons. However, by pulsing on proton during the mixing time we avoid C-H transfer and thereby the relayed magnetization transfer pathway. To confirm that the C-H NOE is indeed properly suppressed we performed an experiment were the proton pulses are given even every 3 ms and same differences in leucine C^{β}-C^{δ} cross-peak intensities are observed for this experiment.

The transfer of magnetization from C^{β} to C^{γ} is equal for both cross-peaks. So the difference must be caused by differences in the transfer of magnetization from C^{γ} to the two methyls. Unfortunately because of overlap we have no information about the direct cross-relaxation rates between C^{γ}-C^{δ} to confirm this independently. The question now rises how can these two pathways be different? One explanation could be that the T_1 relaxation times of the two methyls are very different, causing one of the two NOEs to be scaled down more by T_1, which results in a non-observable cross-peak. However, another explanation is that the motion of the two C^{γ}-C^{δ} pairs is unequal, i.e., that one of the bond vectors is more rigid, which results in the observation of a long-range cross-peak only for that methyl. For the other methyl the order parameter is low, which results in slow cross-relaxation and no observation of a cross-peak. A plausible explanation for differential mobility would be a difference in distance of the two C^{δ} groups from the protein surface. However, no correlation between the solvent accessibility, determined from the crystal structure 1GCI, and the appearance of a C^{β}-C^{δ} cross-peak was found. The absence of a relation between side chain mobility and solvent accessibility has also been reported by others (LeMaster and Kushlan, 1996; Mittermaier et al., 1999).

In contrast to our observations, several studies of methyl-axis order parameters using deuterium relaxation measurements showed generally similar S^2_{axis} values for both leucine methyl groups (Mittermaier et al., 1999; Flynn et al., 2001; Millet et al., 2003). However, differences up to 0.1 in order parameter have been reported, with outliers of even 0.25. More pronounced differences in S^2_{axis} values for the two leucine

Table 1. Long-range cross-peaks for leucines in the 300 ms 3D (H)CCH-NOESY spectrum

		$C^{\beta} \rightarrow C^{\delta 1}$				$C^{\beta} \rightarrow C^{\delta 2}$				$C^{\delta 1} \rightarrow C^{\delta 2}$	$C^{\delta 2} \rightarrow C^{\delta 1}$
	χ_2[b]	NOE	SASA[a]	$\delta(C^{\delta})$	$\delta(H^{\delta})$	NOE	SASA[a]	$\delta(C^{\delta})$	$\delta(H^{\delta})$	NOE	NOE
L21[c]	169.1	–	1.004	20.99	0.803	+	11.715	24.59	0.990	+	[d]
L31	66.5	–	0.000	23.34	0.813	–	0.000	25.49	0.813	[d]	[d]
L41	**173.7**	**+**	**0.000**	**23.80**	**0.704**	–	**0.000**	**20.73**	**0.606**	**+**	**+**
L73	**171.5**	**+**	**22.994**	**24.48**	**0.763**	–	**20.455**	**21.18**	**1.025**	**+**	**+**
L80	**63.6**	–	**0.000**	**20.79**	**0.867**	**+**	**8.792**	**24.79**	**0.965**	**+**	[d]
L88	67.5	+/–	0.000	23.77	0.859	[d]	0.361	22.86	0.791	[d]	[d]
L94	**174.6**	**+**	**5.649**	**23.18**	**0.784**	–	**6.326**	**20.03**	**0.667**	**+**	**+**
L109	**160.6**	**+**	**0.000**	**25.16**	**0.716**	–	**0.000**	**22.07**	**0.739**	**+**	**+**
L122	66.3	+/–	0.000	24.19	0.941	+/–	0.000	25.82	0.824	[d]	–
L124	79.9	+/–	1.488	22.81	0.664	–/+	0.000	26.02	0.800	+	+
L133	59.4	–	0.000	22.17	0.900	–	6.015	23.36	0.960	+	–
L146	**56.6**	–	**3.698**	**21.62**	**1.008**	**+**	**0.000**	**24.68**	**0.854**	[d]	[d]
L190	**62.6**	–	**0.000**	**21.63**	**0.855**	**+**	**0.269**	**27.09**	**0.678**	**+**	**+**
L211	171.6	–	7.084	23.03	0.285	–	48.856	21.24	0.767	–	–
L227	**173.4**	**+**	**0.000**	**23.95**	**0.892**	–	**0.000**	**19.27**	**0.813**	[d]	**+**
L244	**168.1**	**+**	**0.000**	**24.80**	**0.748**	–	**0.161**	**21.42**	**0.654**	[d]	**+**
L251	**–178.3**	**+**	**0.000**	**25.01**	**0.518**	–/+	**13.809**	**20.52**	**0.681**	**+**	**+**
L256	**164.9**	**+**	**43.910**	**23.44**	**0.631**	–	**14.155**	**20.45**	**–0.094**	**+**	**+**
L261[c]	60.1	+	0.000	22.75	0.821	+	12.052	24.96	0.850	+	[d]

[a]Solvent accessible surface area (%) of the C^{δ} atoms calculated from the crystal structure 1GCI.pdb (savinase).
[b]χ_2 angles; an angle close to 180° corresponds to parallel C^{α}-C^{β} and C^{γ}-$C^{\delta 1}$ bonds, an angle close to 60° corresponds to parallel C^{α}-C^{β} and C^{γ}-$C^{\delta 2}$ bonds.
[c]Stereospecific assignment is uncertain.
[d]Overlap with other peaks.

methyls were found in ^{13}C relaxation studies of ubiquitin (Wand et al., 1996) and thioredoxin (LeMaster and Kushlan, 1996; LeMaster, 1999). In the case of ubiquitin the pro-R methyl ($C^{\delta 1}$) consistently has a higher value than the pro-S methyl. For thioredoxin the highest value was found for the pro-S methyl of Leu 99. As is discussed by Lemaster (1999), the majority of leucines in ubiquitin have a χ_2 angle close to 180°, while Leu 99 in thioredoxin has a χ_2 angle close to 60°. Meaning that in both cases the methyl that is trans to the C^{α}-C^{β} bond gives the highest order parameter.

We also found a strong correlation of the cross-peak intensity with the χ_2 angles from the crystal structure, which are listed in Table 1. In case of a χ_2 angle close to 180° the C^{α}-C^{β} and C^{γ}-$C^{\delta 1}$ bonds are parallel and a C^{β}-$C^{\delta 1}$ cross-peak is observed. Similar, a C^{β}-$C^{\delta 2}$ cross-peak is seen for a χ_2 angle of approximately 60°, where the C^{α}-C^{β} and C^{γ}-$C^{\delta 2}$ bonds are parallel as illustrated in Figure 9. This is at least true for 11 of the 12 cases where only one of the two cross-peaks is observed. Only for leucine 21 this was not the case, but the stereo-specific assignment for this residue has been questioned (Karimi, unpublished results). Long-range $^{3}J_{C\alpha C\delta}$ coupling constants (see Supplementary Material to be obtained from the author), which were measured as described by Bax et al. (1992), confirm that the stereo-specific assignment for leucine 21 has to be swapped. The differential mobility can be explained by an anisotropic motion around the axis, which is represented by the dashed lines in Figure 9. In that case the C^{γ}-C^{δ} bond vector that makes an angle of 180° with the C^{α}-C^{β} bond vector, would move in a smaller cone than the other C^{γ}-C^{δ} bond vector. In the shorter side chains of valines this anisotropic motion cannot be present, whereas in other long side chains it would be more difficult to detect due to the asymmetry of the spin-systems. A similar anisotropic motion for the protein backbone has been suggested by Wang et al. (2003) based on ^{13}CO-$^{13}C^{\alpha}$ cross-correlated relaxation rates.

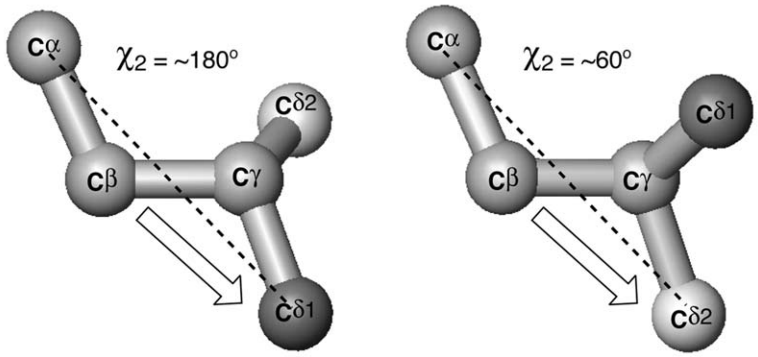

Figure 9. Ball and stick model of the carbon chain of two leucine residues with a χ_2 angle of 180° and 60° degrees, respectively. A correlation was found with the appearance of a long-range C^{β}-C^{δ} cross-peak and the χ_2 angle. For an angle close to 180° a C^{β}-$C^{\delta 1}$ cross-peak is observed and likewise a C^{β}-$C^{\delta 2}$ cross-peak is observed for a χ_2 angle close to 60°. The arrows in the picture indicate the expected cross-peak for the denoted χ_2 angle. This might suggest a difference in mobility for the two methyl groups, caused by a correlated motion around the dashed line.

Conclusions

In this paper we have shown that it is possible to measure ^{13}C-^{13}C cross-relaxation rates for a 269-residue protein, providing that ZQ coherences can be suppressed. These rates are indicative of the motion of the involved C-C pair and can thus be used to probe side chain dynamics in proteins. As expected, the C^{α}-C^{β} cross-relaxation rates from residues located in secondary structure elements indicate on average higher rigidity than those from residues located in loop regions. There is no clear correlation with backbone dynamics extracted from ^{15}N relaxation measurements, which has also been reported by others on the basis of ^{2}H relaxation measurements (Mittermaier et al., 1999). Also more or less expected, the cross-relaxation rates for methyl bearing C-C pairs in the side chains of threonines, valines and isoleucines are on average lower than the average C^{α}-C^{β} rates, indicating increasing mobility further into the side chain. Differences in the two long-range C^{β}-C^{δ} cross-peaks for leucine residues were observed that could be explained by an anisotropic motion in the long side chains of these residues.

The experiment can be applied to fully ^{13}C labeled proteins of considerable size and can therefore be a useful tool to get more insight into the mobility of side chains in proteins.

Acknowledgements

Dr Carine van Heijenoort is gratefully acknowledged for her advices. Dick Schipper provided us with the protein sample. The project was funded by the Netherlands Organization for Scientific Reasearch (NWO).

References

Banci, L., Bertini, I., Felli, I.C., Hajieva, P. and Viezzoli, M.S. (2001) *J. Biomol. NMR*, **20**, 1–10.

Bax, A., Clore, G.M. and Gronenborn, A.M. (1990) *J. Magn. Reson.*, **88**, 425–431.

Bax, A., Max, D. and Zax, D. (1992) *J. Am. Chem. Soc.*, **114**, 6923–6925.

Bodenhausen, G. and Ernst, R.R. (1982) *J. Am. Chem. Soc.*, **104**, 1304–1309.

Boyd, J. (1995) *J. Magn. Reson. Ser. B*, **107**, 279–285.

Brooks, 3rd, C.L., Karplus, M. and Pettitt, B.M. 1988. Proteins, a theoretical perspective of dynamics, structure and thermodynamics, Wiley, New York, 259 pp.

Bystrov, V.F. (1976) *Prog. Nucl. Magn. Reson. Spectrosc.*, **10**, 41–81.

Cain, R.J., Glick, G.D. and Zuiderweg, E.R.P. (1996) *J. Magn. Reson. B*, **113**, 252–5.

Carlomagno, T., Bermel, W. and Griesinger, C. (2003) *J. Biomol. NMR*, **27**, 151–7.

Cavanagh, J., Frairbrother, W.J., Pallmer, A.G. and Skelton, N.J. (1996) *Protein NMR Spectroscopy, Principles and Practice*, Academic Press, San Diego.

Cho, C.H., Urquidi, J., Singh, S. and Robinson, G.W. (1999) *J. Phys. Chem. B*, **103**, 1991–1994.

Cordier, F., Brutscher, B. and Marion, D. (1996) *J. Biomol. NMR*, **7**, 163–168.

Delaglio, F., Grzesiek, S., Vuister, G.W., Zhu, G., Pfeifer, J. and Bax, A. (1995) *J. Biomol. NMR*, **6**, 277–293.

Eisenmesser, E.Z., Bosco, D.A., Akke, M. and Kern, D. (2002) *Science*, **295**, 1520–1523.

Engelke, J. and Rüterjans, H. (1995) *J. Biomol. NMR*, **5**, 173–182.

Engelke, J. and Rüterjans, H. (1998) *J. Biomol. NMR*, **11**, 165–183.

Ernst, M. and Ernst, R.R. (1994) *J. Magn. Reson. Ser. A*, **110**, 202–213.

Fischer, M.W.F., Majumdar, A. and Zuiderweg, E.R.P. (1998) *Prog. Nucl. Magn. Reson. Spectrosc.*, **33**, 207–272.

Fischer, M.W.F., Zeng, L. and Zuiderweg, E.R.P. (1996) *J. Am. Chem. Soc.*, **118**, 12457–12458.
Flynn, P.F., Bieber Urbauer, R.J., Zhang, H., Lee, A.L. and Wand, A.J. (2001) *Biochemistry*, **40**, 6559–69.
Fogh, R.H., Schipper, D., Boelens, R. and Kaptein, R. (1995) *J. Biomol. NMR*, **5**, 259–70.
Frauenfelder, H. (2002) *Proc. Natl. Acad. Sci. USA*, **99**, 2479–2480.
Graycar, T., Knapp, M., Ganshaw, G., Dauberman, J. and Bott, R. (1999) *J. Mol. Biol.*, **292**, 97–109.
Henry, G.D., Weiner, J.H. and Sykes, B.D. (1986) *Biochemistry*, **25**, 590–8.
Jardetzky, O. and Roberts, G.C.K. (1981) In *Molecular Biology*, Press A. (Ed.), New York.
Johnson, B.A. and Blevins, R.A. (1994) *J. Biomol. NMR*, **4**, 603–614.
Kay, L.E., Muhandiram, D.R., Farrow, N.A., Aubin, Y. and Forman-Kay, J.D. (1996) *Biochemistry*, **35**, 361–8.
Kay, L.E., Torchia, D.A. and Bax, A. (1989) *Biochemistry*, **28**, 8972–9.
Kuhn, P., Knapp, M., Soltis, S.M., Ganshaw, G., Thoene, M. and Bott, R. (1998) *Biochemistry*, **37**, 13446–13452.
Lee, A.L., Flynn, P.F. and Wand, A.J. (1999) *J. Am. Chem. Soc.*, **121**, 2891–2902.
Lee, A.L., Urbauer, J.L. and Wand, A.J. (1997) *J. Biomol. NMR*, **9**, 437–440.
LeMaster, D.M. (1999) *J. Am. Chem. Soc.*, **121**, 1726–1742.
LeMaster, D.M. and Kushlan, D.M. (1996) *J. Am. Chem. Soc.*, **118**, 9255–9264.
Lipari, G. and Szabo, A. (1982) *J. Am. Chem. Soc.*, **104**, 4546–4559.
Loh, A.P., Pawley, N., Nicholson, L.K. and Oswald, R.E. (2001) *Biochemistry*, **40**, 4590–4600.
Martin, J.R., Mulder, F.A.A., KarimiNejad, Y., vanderZwan, J., Mariani, M., Schipper, D. and Boelens, R. (1997) *Structure*, **5**, 521–532.
Millet, O., Mittermaier, A., Baker, D. and Kay, L.E. (2003) *J. Mol. Biol.*, **329**, 551–63.
Millet, O., Muhandiram, D.R., Skrynnikov, N.R. and Kay, L.E. (2002) *J. Am. Chem. Soc.*, **124**, 6439–6448.
Mispelter, J., Lefevre, C., Adjadj, E., Quiniou, E. and Favaudon, V. (1995) *J. Biomol. NMR*, **5**, 233–244.
Mittermaier, A., Kay, L.E. and Forman-Kay, J.D. (1999) *J. Biomol. NMR*, **13**, 181–185.
Muhandiram, D.R., Yamazaki, T., Sykes, B.D. and Kay, L.E. (1995) *J. Am. Chem. Soc.*, **117**, 11536–11544.
Mulder, F.A.A., Schipper, D., Bott, R. and Boelens, R. (1999) *J. Mol. Biol.*, **292**, 111–123.
Nicholson, L.K., Kay, L.E., Baldisseri, D.M., Arango, J., Young, P.E., Bax, A. and Torchia, D.A. (1992) *Biochemistry*, **31**, 5253–5263.
Nirmala, N.R. and Wagner, G. (1988) *J. Am. Chem. Soc.*, **110**, 7557–7558.
Palmer, A.G. (2001) *Annu. Rev. Biophys. Biomol. Struct.*, **30**, 129–155.
Palmer, A.G., Rance, M. and Wright, P.E. (1991) *J. Am. Chem. Soc.*, **113**, 4371–4380.
Peng, J.W. and Wagner, G. (1994) In *Investigation of Protein Motions via Relaxation Measurements. Nuclear Magnetic Resonance, Part C*, Academic Press Inc., San Diego, pp. 563–596.
Ramirez-Alvarado, M., Daragan, V.A., Serrano, L. and Mayo, K.H. (1998) *Protein Sci.*, **7**, 720–729.
Rance, M., Bodenhausen, G., Wagner, G., Wüthrich, K. and Ernst, R.R. (1984) *J. Magn. Reson.*, **62**, 497–510.
Remerowski, M.L., Pepermans, H.A.M., Hilbers, C.W. and VandeVen, F.J.M. (1996) *Eur. J. Biochem.*, **235**, 629–640.
Shaka, A.J., Lee, C.J. and Pines, A. (1988) *J. Magn. Reson.*, **77**, 274–293.
Siezen, R.J. and Leunissen, J.A.M. (1997) *Protein Sci.*, **6**, 501–523.
Siezen, R.J., Devos, W.M., Leunissen, J.A.M. and Dijkstra, B.W. (1991) *Protein Eng.*, **4**, 719–737.
Skrynnikov, N.R., Millet, O. and Kay, L.E. (2002) *J. Am. Chem. Soc.*, **124**, 6449–6460.
States, D.J., Haberkorn, R.A. and Ruben, D.J. (1982) *J. Magn. Reson.*, **48**, 286.
Walsh, S.T.R., Lee, A.L., DeGrado, W.F. and Wand, A.J. (2001) *Biochemistry*, **40**, 9560–9569.
Wand, A.J., Bieber, R.J., Urbauer, J.L., McEvoy, R.P. and Gan, Z.H. (1995) *J. Magn. Reson. Ser. B*, **108**, 173–175.
Wand, A.J., Urbauer, J.L., McEvoy, R.P. and Bieber, R.J. (1996) *Biochemistry*, **35**, 6116–25.
Wang, T.Z., Cai, S. and Zuiderweg, E.R.P. (2003) *J. Am. Chem. Soc.*, **125**, 8639–8643.
Yamazaki, T., Muhandiram, R. and Kay, L.E. (1994) *J. Am. Chem. Soc.*, **116**, 8266–8278.
Yang, D., Mittermaier, A., Mok, Y.K. and Kay, L.E. (1998) *J. Mol. Biol.*, **276**, 939–54.
Zeng, L., Fischer, M.W.F. and Zuiderweg, E.R.P. (1996) *J. Biomol. NMR*, **7**, 157–162.
Zwahlen, C., Legault, P., Vincent, S.J.F., Greenblatt, J., Konrat, R. and Kay, L.E. (1997) *J. Am. Chem. Soc.*, **119**, 6711–6721.